Hindawi
International Journal of Antennas and Propagation
Volume 2018, Article ID 1905984, 16 pages
https://doi.org/10.1155/2018/1905984

Research Article

Watchstrap-Embedded Four-Element Multiple-Input–Multiple-Output Antenna Design for a Smartwatch in 5.2–5.8 GHz Wireless Applications

Chia-Hao Wu, Jwo-Shiun Sun, and Bo-Shiun Lu

Department of Electronic Engineering, National Taipei University of Technology, 1 Sec. 3, Zhongxiao E. Rd., Taipei 10608, Taiwan

Correspondence should be addressed to Chia-Hao Wu; chwu.tpc@gmail.com

Received 15 October 2017; Revised 3 February 2018; Accepted 20 February 2018; Published 18 April 2018

Academic Editor: Miguel Ferrando Bataller

This paper presents a compact four-element multiple-input–multiple-output (MIMO) antenna design operating within the WiFi 802.11 ac bands (5.2–5.84 GHz) for a smartwatch. The antenna is fabricated using a polyamide substrate and embedded into the strap of a smartwatch model; the strap is created using three-dimensional etching of plastic materials. The four-element MIMO antenna is formed by four monopole antennas, has a simple structure, and is connected to the system ground plane of the smartwatch. Due to the stub and notched block between two antennas and the slit in the system ground, the four-element MIMO antenna exhibits favorable isolation. Moreover, the envelope correlation coefficient of the antennas is considerably lower than 0.005 in the operating band. The measured −6 dB impedance bandwidths of the four elements of the antenna (Ant1–Ant4) with the human wrist encompass the WiFi 802.11 ac range of 5.2–5.84 GHz; moreover, an isolation of more than 20 dB is achieved. The measured antenna efficiency with and without a phantom hand are 45%–55% and 93%–97%, respectively.

1. Introduction

Forty years after the revolutionary development of personal computing that occurred in the 1970s, the technological world is experiencing a second revolution—the Internet of Things—which has applications in various domains, such as smart homes, medicine, fitness, and gaming. In particular, wearable devices, such as smartwatches, smartglasses, and virtual-reality headsets, are set to lead the economic development of the Internet of Things. For example, wearable products are ideal for conveniently controlling any device in smart homes. The Internet of Things is a human-centric concept, and wearable products are part of the relationship between human users and intelligent home appliances. Currently, mobile devices such as smartphones can be employed to control home appliances. However, wearable controllers, such as smartwatches, can increase the convenience of and reduce the time required for operating home appliances, thus greatly enhancing user experience. Wearable wireless devices are finding increasing applications such as in heart rate control, the sending and receiving of emails and multimedia files, the answering of mobile phone calls, and the tracking of user devices. To enable smartwatches to play a crucial role in the Internet of Things, the wireless communication transmission capacity must be upgraded. Multiantenna designs can be used to attain this objective; for example, wireless WiFi AP employs multiple-input–multiple-output (MIMO) multiantennas to achieve high-transmission speed. Moreover, the WiFi 802.11 ac specification supports an 8×8 antenna, which greatly enhances the transmission speed in MIMO transmitter antennas. MIMO antennas have been designed for WiFi 802.11 ac, the advantage of which is high-transmission speed. The transmission speed of WiFi 802.11 ac is three times higher than that of the previous generation, WiFi 802.11n. WiFi 802.11 ac has a bandwidth of 80 MHz, operates at 5 GHz, and can reduce interference of the 2.45 GHz frequency band. Currently, smartwatch antennas are positioned under the LCD panel or around the main body of the watch (e.g., in an Apple Watch), and WiFi band and Bluetooth antennas are inserted into space of limited size. A multiantenna design cannot be employed due to the limited volume of the host object [1–3]. Several studies on MIMO

antennas have proposed the implementation of the antenna on the host object of a smart watch [4–6]; however, those studies were conducted for the 2.4 GHz band and did not specify the antenna efficiency. An antenna [7] was designed for the 2.4 and 5.2 GHz bands but managed to only provide the simulated efficiency of the 2.4 GHz band. A circular slot antenna for 2.4 GHz WLAN on a watchstrap has been investigated [8].

This paper proposes a polyamide substrate-based four-element MIMO antenna that can be embedded in the plastic watchstrap of a smartwatch device for use in 5.2–5.84 GHz wireless applications. The polyamide substrate of the antenna is suitable for use in soft electronics, is built on a flexible substrate film, and is light, flexible, low cost, and robust [9–12]. The biggest advantage of soft electronics is their ability to bend because curved features enable devices to fit the human body closely. Wearable devices, such as smart watches, smart glasses, and smart clothing, have great potential in benefiting human life in numerous ways. The proposed multiantenna, which comprises four flexible antennas, is positioned over a smartwatch strap for optimal use of the wearable watch. A design in which the MIMO antenna is isolated is crucial for high performance. Therefore, studies have explored MIMO antenna decoupling technology to improve the methods of isolating MIMO antennas, such as stub [13–16], defected ground structure [17, 18], neutralization line [19, 20], electromagnetic band gap [21], and polarization [22–25] methods. The stub and notched block designs are used in the present study to reduce the pattern field overlapping between the four elements in the MIMO antenna, that is, between Ant1 and Ant2 and between Ant3 and Ant4. The details of the proposed antenna and its performance in the WiFi band are discussed in the following sections.

2. Antenna Design

Figure 1(a) illustrates the four-element MIMO antenna attached to the watchstrap of a smartwatch model. The watchstrap and smartwatch model are created using a three-dimensional etching process for plastic materials. The material is photopolymer resin with a dielectric constant of 3. The back-cover size of the smartwatch model is $40 \times 38 \times 8\ \text{mm}^3$, and the thickness and width of the watchstrap are 3.8 and 25 mm, respectively. To practically simulate strap bending, the bend shape of the smartwatch strap is set to that of a normal-sized plastic strap. We set the angle θ to 30° in the curved design because watches are generally worn on the wrist at this angle. The MIMO antenna Ant1–Ant4 is fed by the port 1–port 4, respectively.

The geometry of a two-element MIMO antenna is presented in Figure 1(b). The four-element MIMO antenna is printed on a 0.135 mm thick polyamide substrate (dielectric constant: 4.3; loss tangent: 0.004), and the antenna is fed by the coplanar waveguide (CPW). The ground of the four-element MIMO antenna is connected to the system ground through eight via holes; the system ground is on the back surface of the system circuit board. Moreover, four via holes connect each side of the polyamide substrate and FR4 substrate. A system circuit board of size $30 \times 35\ \text{mm}^2$ is selected and is fabricated using a 0.4 mm thick FR4 substrate (relative permittivity: 4.4; loss tangent: 0.02). The optimized dimensions (in mm) of the proposed structures are as follows: $W = 25$, $L = 20$, $G_y = 7.5$, $G_p = 0.25$, $G_x = 5$, $W_s = 1$, $L_s = 8$, $W_1 = 1.5$, $L_1 = 10$, $D_L = 4$, and $D_w = 2$. The size of the slit into the system ground is $2.0 \times 8.5\ \text{mm}^2$ ($S_g \times S_w$), and the distance between the antenna and the circuit board edge is 3 mm (S_d). The slit is employed to decrease mutual coupling between Ant1 and Ant4 and between Ant2 and Ant3. The length of the antenna (L_s) is designed to be 0.15 wavelength in the 5.5 GHz band when the MIMO antenna is attached to the watchstrap of the smartwatch model. The ground stub and notched block of the MIMO antenna are used to decrease mutual coupling between Ant1 and Ant2 and between Ant3 and Ant4. Figure 1(c) displays the side view of the polyamide substrate and FR4 substrate, which are connected using a shorting pin with 0.6 mm diameter via holes. Figure 1(d) displays a photograph of the MIMO antenna. The two elements of the MIMO antenna are mounted at opposite ends of the smartwatch model. The MIMO antenna is fed by 50 Ω mini coaxial lines connected to the feeding point (ports 1–4).

3. Results and Discussion

3.1. Effect of the Notched Block and Stub for the Two-Element MIMO Antenna. The S-parameters of the two-element MIMO antenna are determined using the high-frequency structural electromagnetic field simulator (HFSS, ANSYS, Canonsburg, PA, USA), which is based on the finite element method. Figures 2(a) and 2(b) display the S-parameters (S_{21} and S_{11}) for the MIMO antenna with or without the notched block and stub when the antenna only has two elements and is not bent in free space. Figure 2(c) presents the various MIMO antenna structures used—the ground of the MIMO antenna with the stub and notched block (MIMO antenna A), antenna with the stub but without the notched block (MIMO antenna B), and antenna without both the stub and notched block (MIMO antenna C). The MIMO antennas A, B, and C are not combined with the watchstrap and are not connected to the system ground. The length of the antenna (*Ls*) is designed to be one quarter of λ_g at 5.5 GHz. The dimensions (in mm) of the two-element MIMO antenna are $W = 25$, $L = 20$, $G_y = 7.5$, $G_p = 0.25$, $G_x = 5$, $W_s = 1$, $L_s = 13.9$, $W_1 = 1.5$, $L_1 = 11$, $D_L = 1$, and $D_w = 2$. As the S-parameter (S_{11}) is less than −10 dB, the bandwidth of MIMO antenna A is wider than that of MIMO antennas B and C; however, the parameter S_{21} is higher than −20 dB. MIMO antenna C is more isolated than MIMO antennas A and B, as shown in Figure 2(b). The stub between the two elements of the MIMO antenna is used to increase the isolation. The notched block is employed to achieve the 5.2–5.84 GHz bandwidth (Figure 2(a)).

3.2. Results of the Two-Element MIMO Antenna. The S-parameters of the two-element MIMO antenna with or without the watchstrap are measured using an N9019A EXA Signal Analyzer (Agilent). First, the two-element MIMO antenna is not combined with the system ground and the smartwatch back cover. Figure 3(a) illustrates the

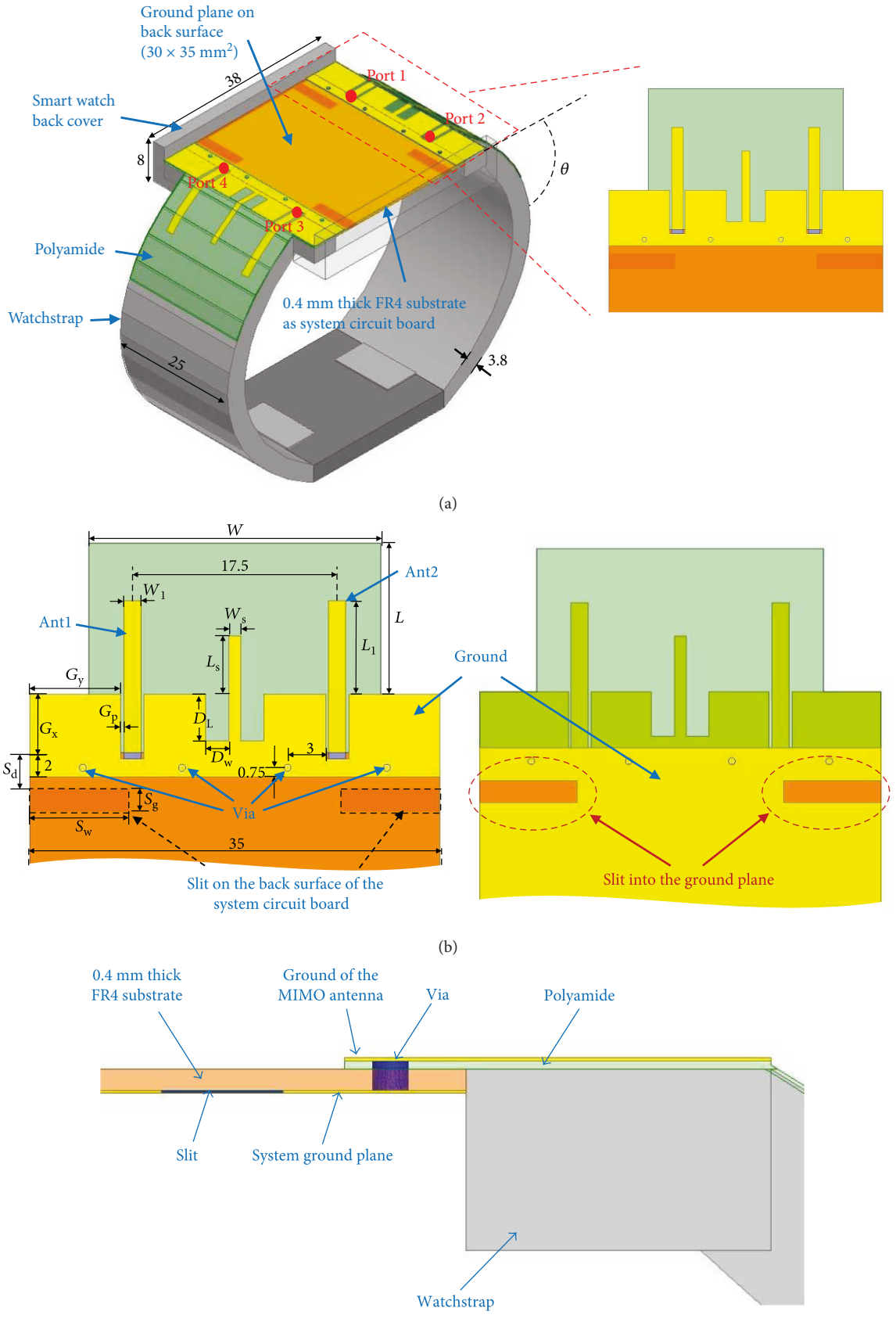

Figure 1: Continued.

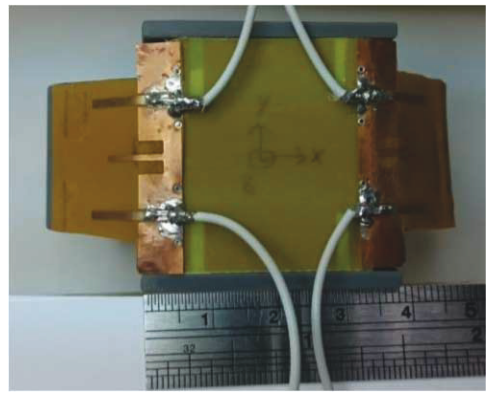

(d)

Figure 1: (a) Four-element MIMO antenna embedded in the smartwatch model. (b) Configuration, (c) side view, and (d) photograph of the MIMO antenna.

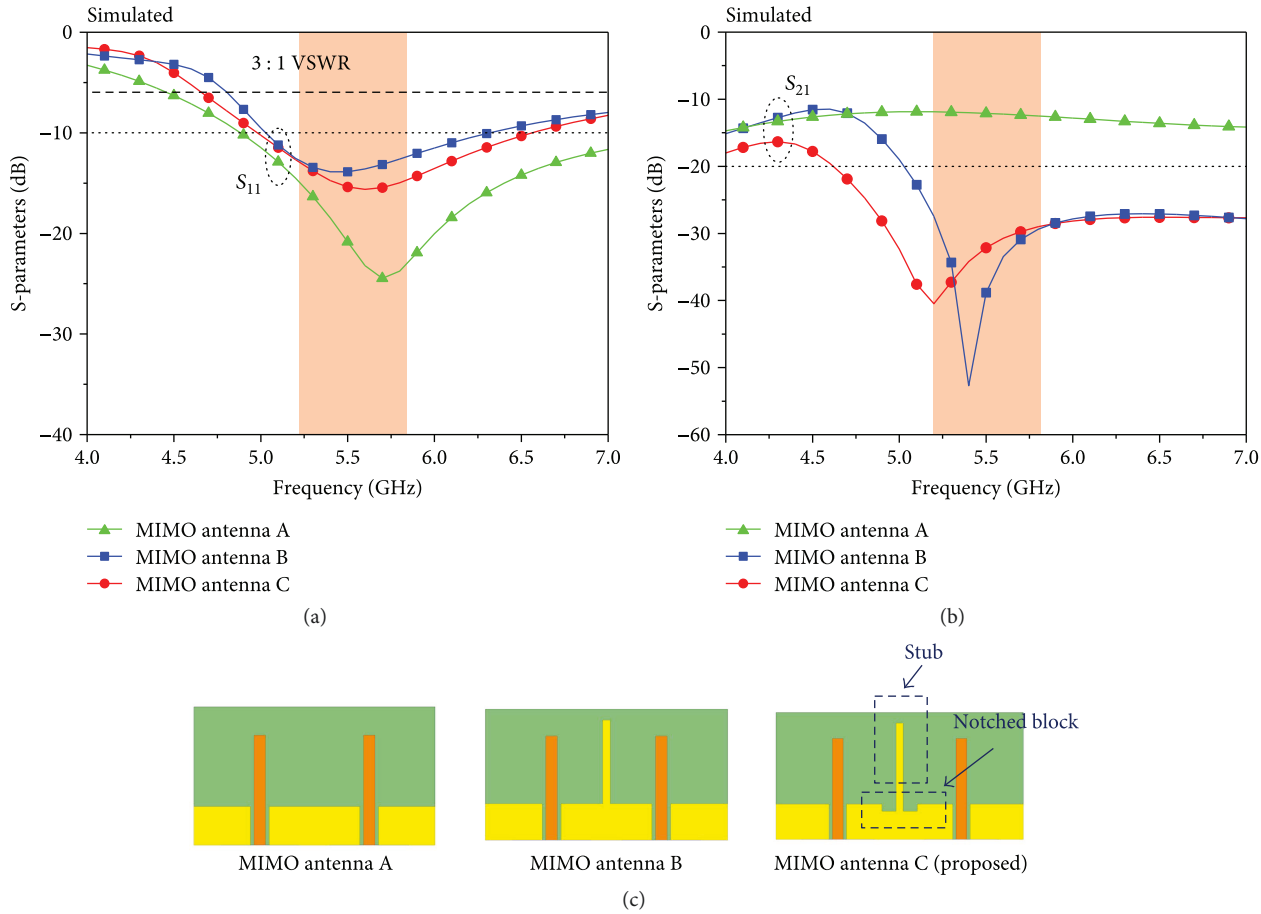

Figure 2: (a) S_{11} and (b) S_{21} parameters of the MIMO antenna with or without the stub and notched block. (c) Various MIMO antenna structures.

configuration of the two-element MIMO antenna bent at an angle of θ in free space. Figure 3(b) presents the measured S_{11} and S_{21} parameters of the two-element MIMO antenna when the antenna is bent at various angles (0°, 30°, 45°, and 70°) in free space (i.e., without a plastic strap). When the two-element MIMO antenna is bent in free space, the original frequency band of 5, 6 GHz becomes offset to a higher frequency due to the increase in θ. Figure 3(c) presents the measured radiation patterns of E-phi for the MIMO antenna (Ant1) bent at 0°, 30°, 45°, and 70°. Waves are present in the measured patterns because the antenna is placed into styrofoam that is cut at different angles. Moreover, the

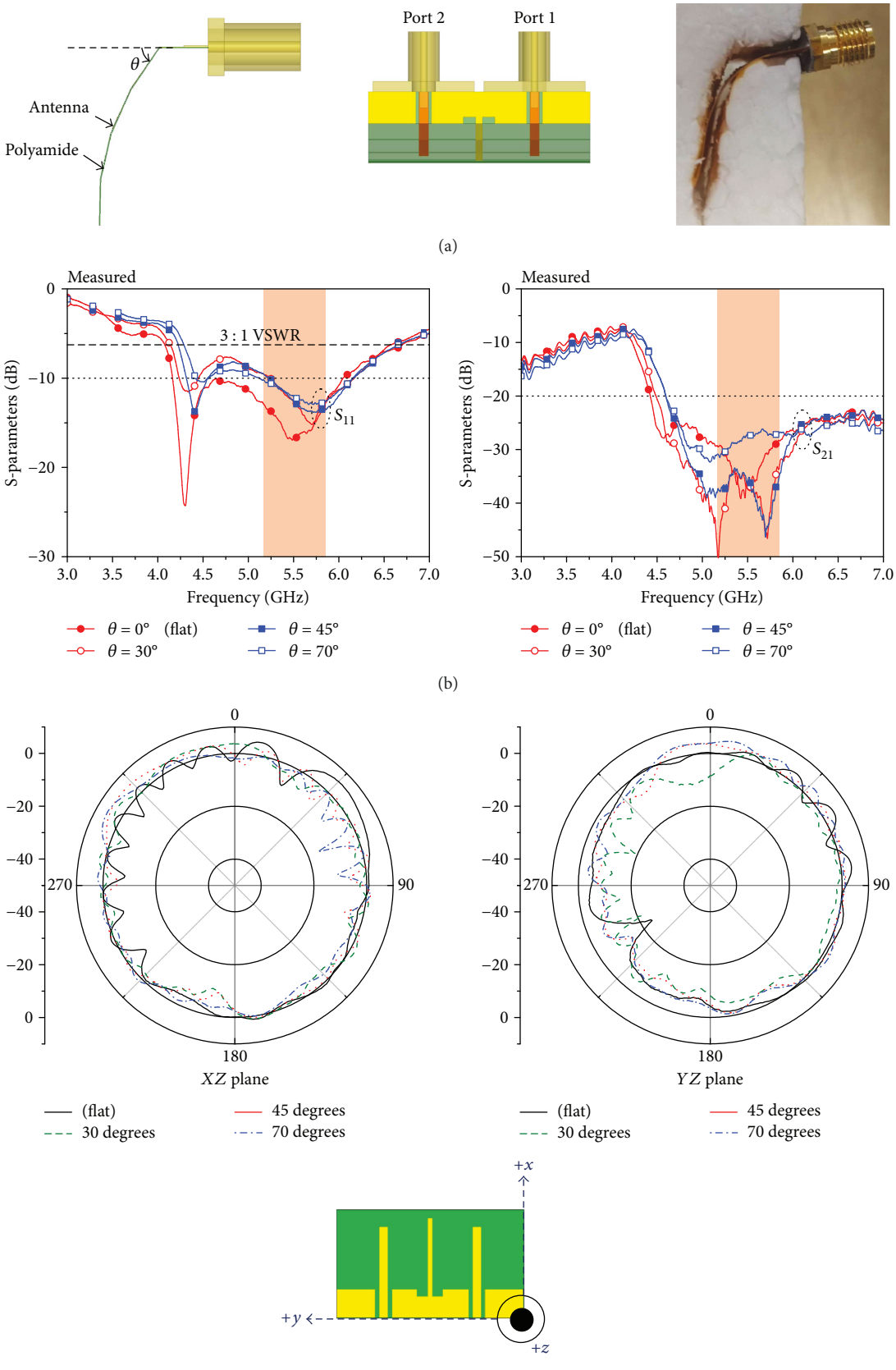

Figure 3: Continued.

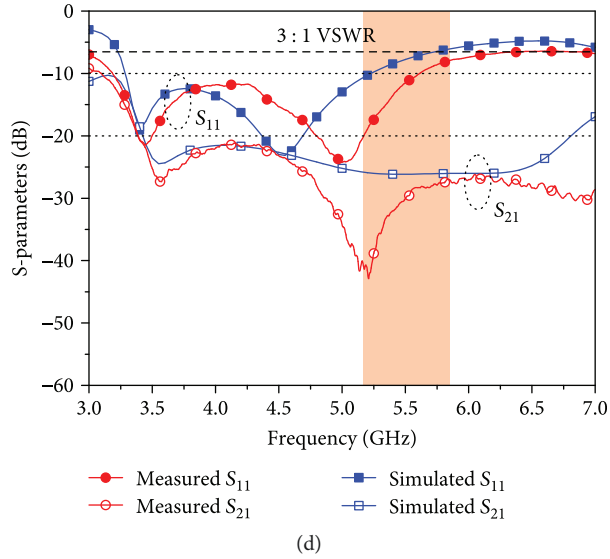

Figure 3: (a) Configuration of the two-element MIMO antenna at angle θ in free space. (b) Measured $S11$ and $S21$ at different degrees of bending for the two-element MIMO antenna in free space. (c) Measured radiation pattern for the two-element MIMO antenna bent at different angles in free space. (d) Measured and simulated $S11$ and $S21$ at the bending angle of 30° with the watchstrap for the MIMO antenna.

polyamide substrate surface becomes nonuniform because the surface is very thin. For each bending angle, the radiation pattern in the YZ plane was stronger at 90° than at 270°; this is because the radiation pattern was measured at port 1, which is at the $+Y$ orientation. The proposed MIMO antenna radiation performance did not change at different angles in free space. The radiation pattern is substantially affected by the bending angle. Figure 3(d) displays the measured and simulated S-parameters for the two-element MIMO antenna at the bending angle of 30° with the watchstrap. At a measured S-parameter (S_{11}) of −6 dB [3 : 1 voltage standing wave radio (VSWR)], the bandwidth is 3500 MHz (3–6.5 GHz; approximately 73.7%). The bandwidth obtained from simulation is 2600 MHz (3.25–5.85 GHz; approximately 57.1%). The measured and simulated S_{11} are compared; the measured first resonant mode is approximately similar to the simulated first resonant mode. However, the measured second resonant mode is shifted to a higher frequency. Furthermore, the simulated and measured S_{21} exceed 20 dB between 5.2 and 5.84 GHz. Figure 4 displays the measured S-parameters of the two-element MIMO antenna at a bending angle of 30° with and without the watchstrap. The bandwidth of the MIMO antenna with the watchstrap is 3500 MHz (3–6.5 GHz; approximately 73.7%), and the bandwidth of the MIMO antenna in free space is 2485 MHz (4.125–6.61 GHz; approximately 46.2%). When the MIMO antenna is attached to the watchstrap (i.e., not including the smartwatch back cover), the first resonant mode of the S-parameter (S_{11}) shifts from 4.3 to 3.4 GHz and the second resonant mode shifts from 5.8 to 5.2 GHz. Obviously, the overall S-parameters shift to a lower frequency. The polyamide substrate (dielectric constant: 4.3) is combined with the photopolymer resin (dielectric constant: 3), and the two materials' different dielectric constants affect the antenna and shift the resonant mode to a lower frequency. Therefore, the length of the

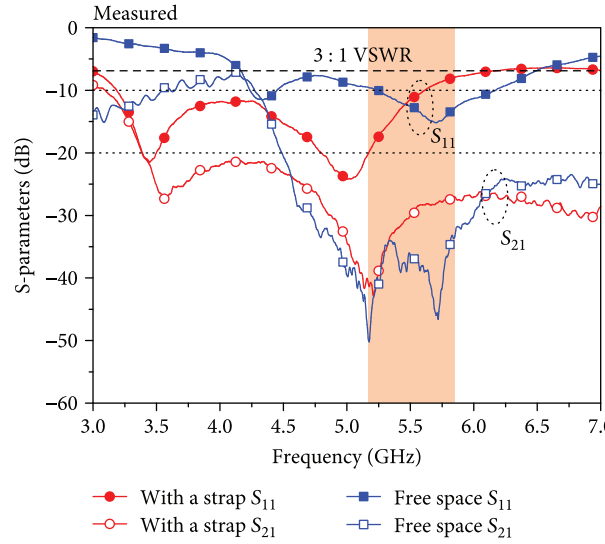

Figure 4: Measured S-parameters of the two-element MIMO antenna at the bending angle of 30° with and without the watchstrap.

antenna (L_s) can be set to be less than a quarter of λ_g in the 5.5 GHz band.

3.3. Effects of the Slit into the System Ground for the Four-Element MIMO Antenna. The four-element MIMO antenna is attached to the smartwatch model, and the two elements of each antenna are connected to the system ground using four via holes. The smartwatch model consists of two watchstraps and a back cover, as shown in Figure 1(d). The simulated S-parameters of the MIMO antenna transformed when a slit was modified in the system ground, as shown in Figure 5. The length of the slit (S_w) is increased from 6.5 to

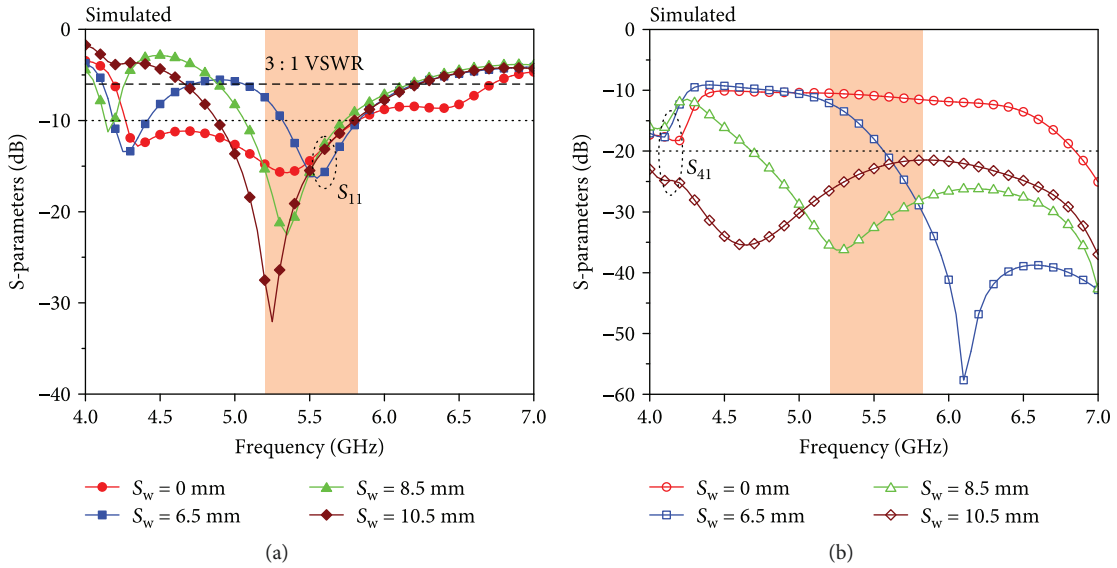

Figure 5: Simulated S-parameters of the antenna with the slit in the system ground: (a) $S11$ and (b) $S41$.

10.5 mm, and the length is 0 mm when the system ground has no slit. The resonance frequency of the S-parameters (S_{11} and S_{41}) both shift to a higher frequency when S_w is increased. As S_w is varied, S_{11} remains lower than −6 dB in the operating band. However, S_{41} is larger by approximately −10 dB when S_w is 0 mm. The slits in the system ground are used to improve S_{41} between Ant1 and Ant4. Thus, the isolation between Ant2 and Ant3 improves effectively.

3.4. Effects of the Via for the Four-Element MIMO Antenna. The ground of the MIMO antenna is connected to the system ground, which is on the back surface of the system circuit board, through the via holes. Moreover, these four via holes connect each side of the polyamide substrate and FR4 substrate. The structures obtained when employing four via holes and two via holes are illustrated in Figure 6(a). The simulated S_{11} and S_{21} are plotted in Figure 6(b).

S_{21} of the ground of the MIMO antenna connected to the system ground through two via holes is larger than −20 dB in the operating band of 5.2–5.84 GHz. Figure 6(c) illustrates the simulated S_{31} and S_{41}, which are unaffected by the number of via holes. Figure 6(d) displays the simulated surface current distributions over the four via holes and two via holes at 5.8 GHz. The four via holes of the two-element MIMO antenna are used to connect the polyamide substrate and system ground. Therefore, the surface current distributions are more uniform from the MIMO antenna ground to the system ground plane when four via holes are used compared with two, and a strong surface current on the stub is observed. This strong surface current improves the isolation of the S-parameter (S_{21}).

3.5. Results of the Four-Element MIMO Antenna in Free Space. The S-parameters of the four-element MIMO antenna connected to the smartwatch model are measured using the N9019A EXA Signal Analyzer and are simulated using the aforementioned HFSS. During the measurements, ports 1 and 2 are excited and the other ports are terminated using a 50 Ω load. Figures 7(a) and 7(b) present the measured and simulated S-parameters of the proposed MIMO antenna. Figure 7(a) displays that the measured S-parameters S_{11}, S_{22}, S_{33}, and S_{44} are less than −6 dB (3 : 1 VSWR) in the desired frequency range of 5.2–5.84 GHz, and S_{21}, S_{31}, and S_{41} are less than −20 dB over the entire operational band. Figure 7(b) demonstrates that the bandwidth of the simulated S_{11}, S_{22}, S_{33}, and S_{44} is approximately 1420 MHz (4.8–6.2 GHz; approximately 25%); moreover, the simulated S_{21}, S_{31}, and S_{41} are less than −20 dB over the entire operational band. The impedances of the measured S_{11}, S_{22}, S_{33}, and S_{44} differ slightly because the MIMO antenna is bent on the watchstrap; nevertheless, the bandwidth of S_{11}, S_{22}, S_{33}, and S_{44} covers the operation frequency.

For a complete investigation of the far-field performance of the MIMO antenna inside an anechoic chamber, an N5230A vector network analyzer (Agilent) and computer workstation running 3D NSI 800F far-field measurement software are used according to generally applied methodologies to measure antenna gain and efficiency. The measured and simulated antenna efficiencies and peak gains for the four-element MIMO transmit ports (Ant1–Ant4) are presented in Figure 8. As shown in Figure 8(a), the measured efficiencies of Ant1–Ant4 are approximately 93%–97% in the operation band and the measured peak gains of Ant1–Ant4 are approximately 3.35–5.6 dBi. In addition, the simulated antenna efficiencies are between 94% and 97% in the operation band and the simulated peak gains are approximately 3.6–4.6 dBi (Figure 8(b)). The simulation efficiency is calculated using the finite element method (HFSS); the efficiency of the antenna located in free space is calculated using pattern integration. In this method, the radiation efficiency is the ratio of the radiated power to the accepted power [26]. The simulation results are in agreement with

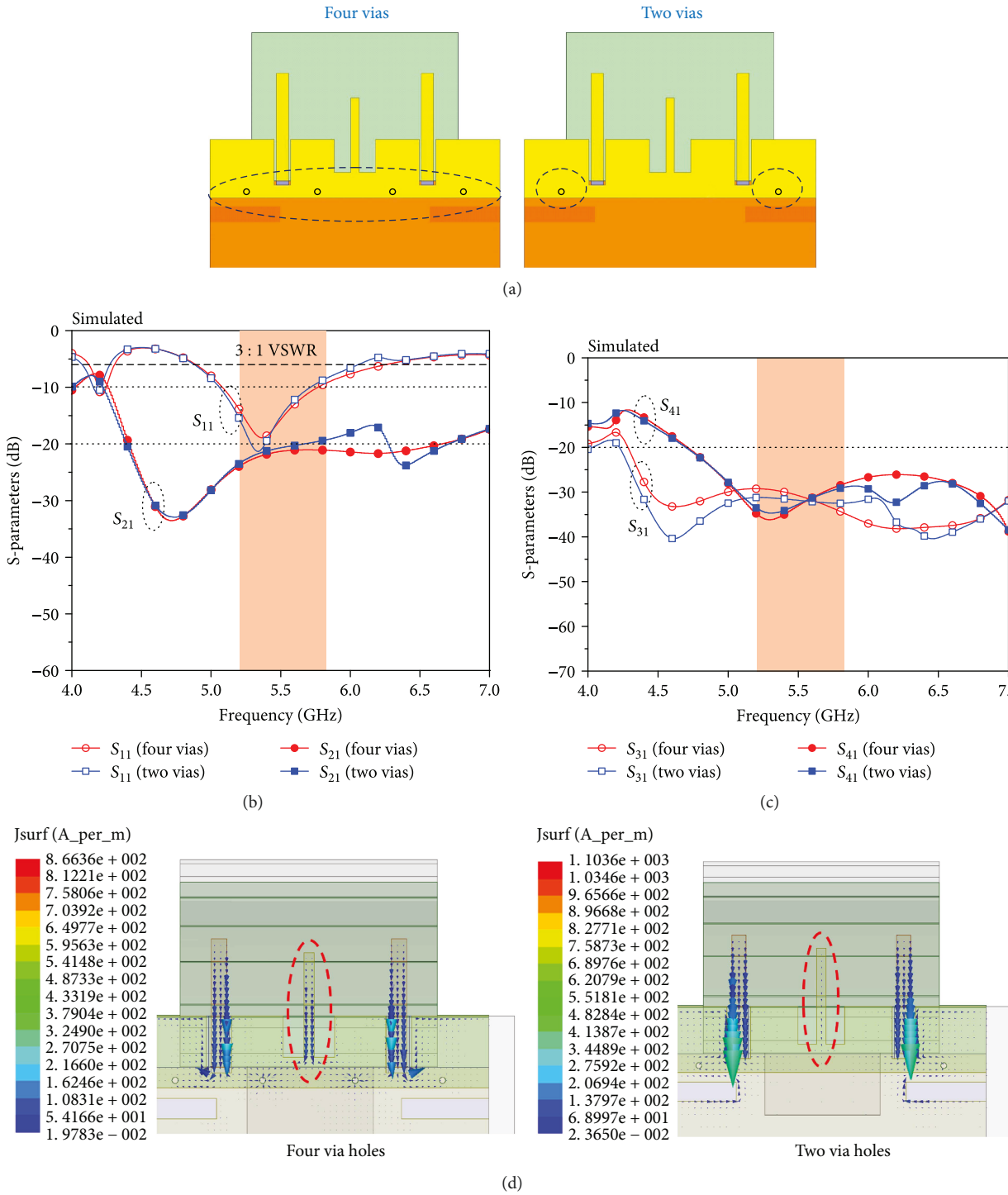

FIGURE 6: (a) Structures with four and two via holes. (b) Simulated *S*11 and *S*21 and (c) *S*31 and *S*41 for the four-element MIMO antenna with via holes. (d) Simulated surface current distributions over the four and two via holes at 5.8 GHz.

the measured results. The antenna has reasonable and stable efficiency in the operation band, making the antenna suitable for practical applications.

Figures 9(a) and 9(b) display the 3D measured and simulated radiation patterns for the four-element MIMO antenna at 5.5 GHz, respectively. Figure 9(c) presents the 2D measured radiation patterns for the MIMO antenna. The Ant1 and Ant2 simulated radiation patterns are in agreement with the measured radiation patterns. The strongest radiating direction of Ant1 lies between the positive *x*-axis and positive *y*-axis, and that for Ant2 lies between the positive *x*-axis and negative *y*-axis. The radiating direction is affected by the stub and notched block in the ground that are designed between the two elements of the antenna.

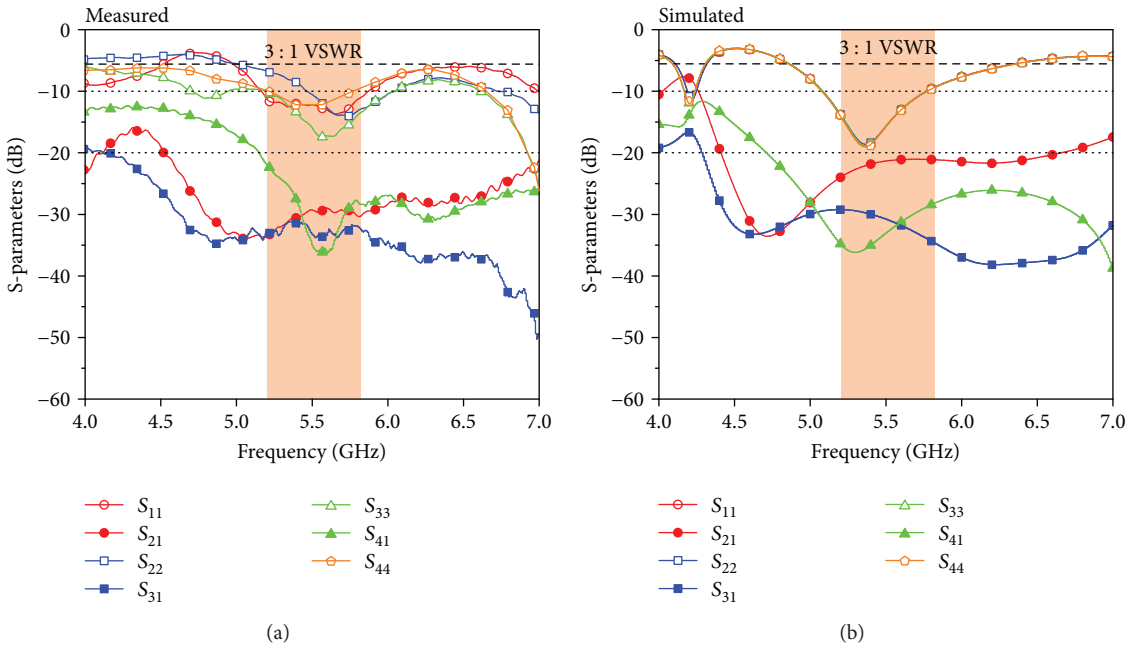

Figure 7: (a) Measured and (b) simulated S-parameters of the four-element MIMO antenna in free space.

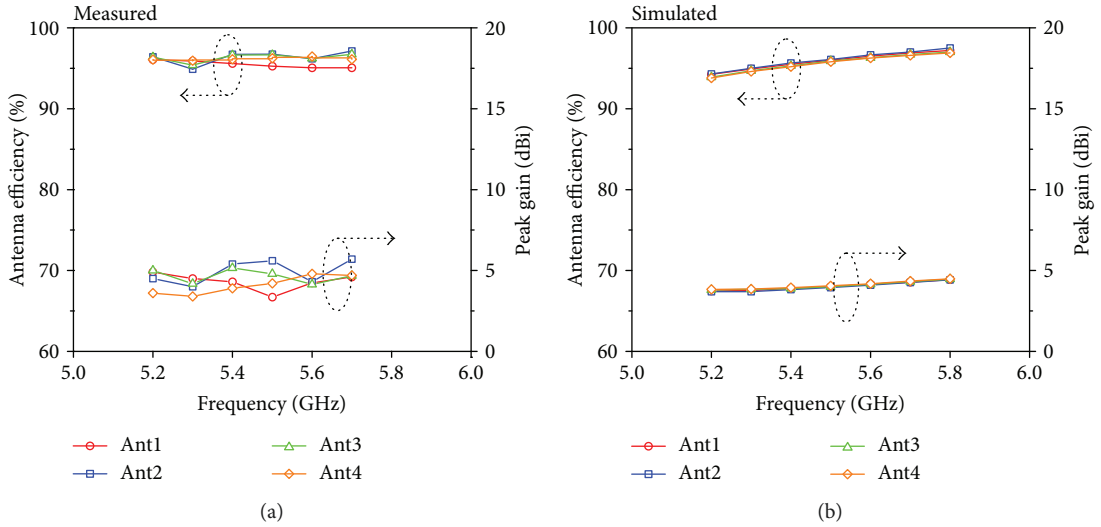

Figure 8: (a) Measured and (b) simulated antenna efficiencies and peak gains of the four-element MIMO antenna.

To verify the suitability of the proposed antenna for MIMO applications, a low envelope correlation coefficient (ECC) is necessary. The ECC describes the extent to which the communication channels are isolated or correlated with each other. The ECC can be evaluated using the equation mentioned in [27]. Figure 10(a) displays the ECC calculated from the measured complex electric-field patterns for Ant1–Ant4 in the MIMO antenna. Superior ECCs for any two antennas within the MIMO antenna are obtained. All ECCs are less than 0.05 in the operation band. The simulated ECCs of the two antennas obtained from the complex radiation patterns [28, 29] are presented in Figure 10(b). All obtained ECCs are considerably lower than 0.01 in the operation band, which is desirable for MIMO operation.

3.6. Results of the Four-Element MIMO Antenna with the Wrist. Simulation configurations with a wrist model are considered because the four-element MIMO antenna is a wearable antenna, as illustrated in Figure 11(a). Phantoms used in some studies have been skin, muscle, and bones [30, 31]. Other studies have only used bone phantoms [32] and hand-tissue-equivalent medium phantoms [33]. The *Regional Anatomy and Surgical Intervals* [34] suggests that the wrist primarily comprises bones, with very less muscle content. Utilizing a cross section of a wrist for the study is complex and inconvenient. A study, *RF/Microwave Interaction with Biological Tissues* [35], suggested that the relative permittivity and conductivity constants can be controlled by varying the mixture rate of silicone emulsion in the

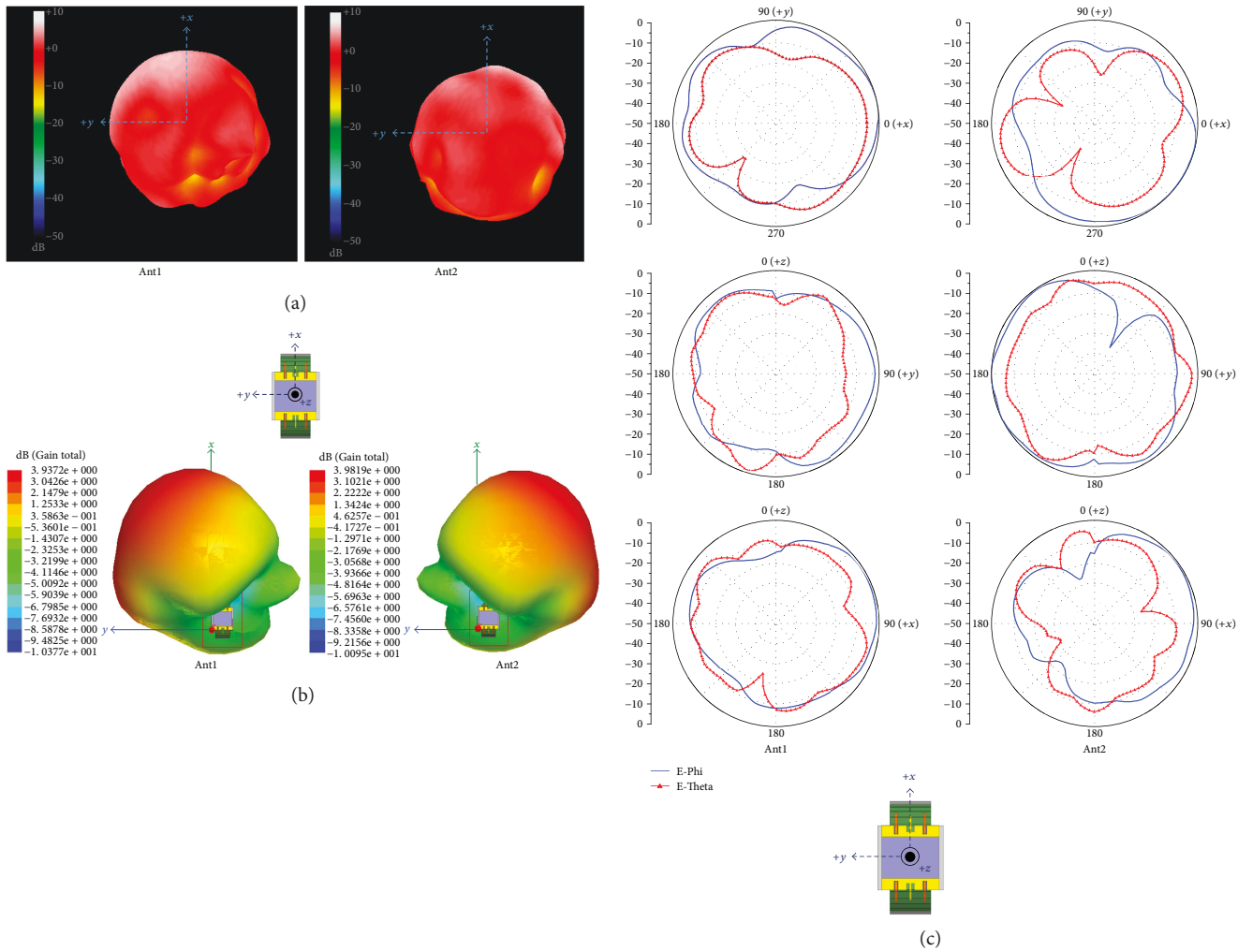

Figure 9: (a) Measured and (b) simulated 3D radiation patterns for the four-element MIMO antenna in free space (at 5.5 GHz). (c) Measured 2D radiation patterns (at 5.5 GHz).

skull-equivalent phantom composition. In the present study, the material of the bone-equivalent phantom hand contains a huge amount of silicone (relative permittivity: 18.6; conductivity: 0.8 S/m). Moreover, we used a 1 mm thick artificial skin to cover the phantom. By referring to the artificial phantoms employed in [36, 37], the dry skin for the frequency range of 0.5–10 GHz in that study is presented such that it has relative permittivity and conductivity approximately in the ranges of 45–31.4 and 0.73–8 S/m, respectively. The artificial skin is made of hydrocolloid thin dressing materials that have good conductivity. Therefore, we use skin and bone equivalent in the simulation in this study. The results thus obtained are similar to those of the measurement of a human hand. The wrist model is composed of skin (relative permittivity: 38; conductivity: 1.4 S/m) and bone equivalent (permittivity: 18.6; conductivity: 0.8 S/m) [8]. The thickness of the skin used is 1 mm, and the long axis and short axis of the bone equivalent used are 60 and 41 mm, respectively. Figure 11(b) illustrates the measurement of the S-parameters of the antenna on the watchstrap connected to the human wrist using the vector network analyzer. For a complete investigation of the far-field performance of the proposed MIMO antenna inside an anechoic chamber, an N5230A vector network analyzer (Agilent) and computer workstation running 3D NSI 800F far-field measurement software are used according to generally applied methodologies to measure antenna gain and efficiency. Figure 11(c) displays a photograph of measurements using a phantom hand in an anechoic chamber.

Figure 12(a) presents the S-parameters of the four-element MIMO antenna that is attached to the smartwatch model and mounted on the human wrist. The measured S_{11}, S_{22}, S_{33}, and S_{44} of the four-element transmit ports are less than −6 dB (3 : 1 VSWR) in the 5.2–5.84 GHz band. Typically measured S_{21}, S_{31}, and S_{41} between Ant1 and the three nearby ports (Ant2, Ant3, and Ant4) are also shown and are less than −20 dB in the 5.2–5.8 GHz band. Figure 12(b) illustrates the simulated S-parameters of the four-element MIMO antenna with the wrist model. S_{11}, S_{22}, S_{33}, and S_{44} are less than −6 dB in the desired frequency range of 5.2–5.84 GHz. Furthermore, S_{21}, S_{31}, and S_{41} are less than −20 dB over the entire operational band.

Figures 13(a) and 13(b) display a comparison of the S-parameters obtained when simulation is conducted by using

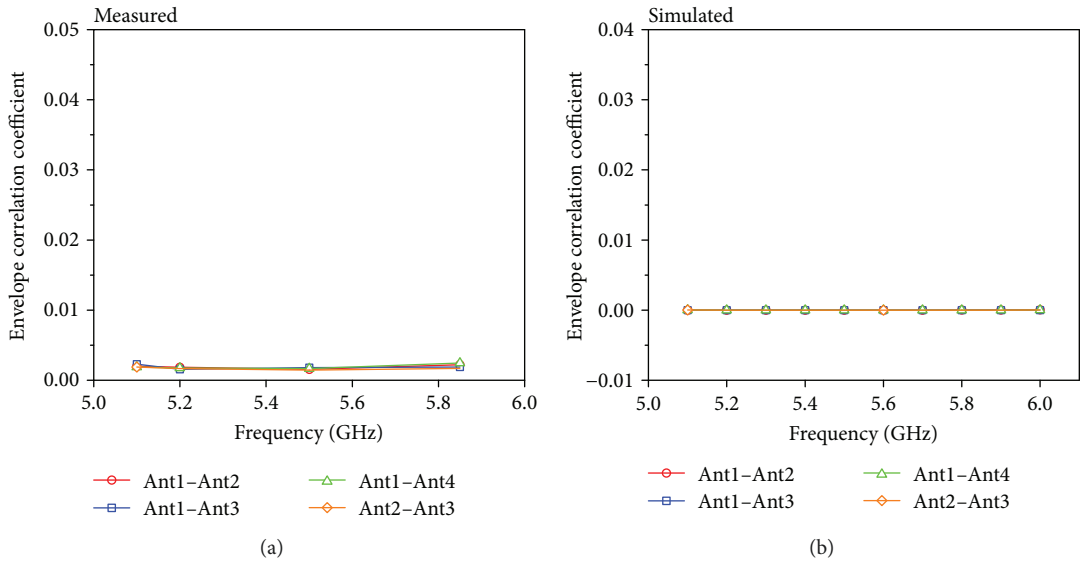

FIGURE 10: (a) Measured and (b) simulated ECCs of the four-element MIMO antenna.

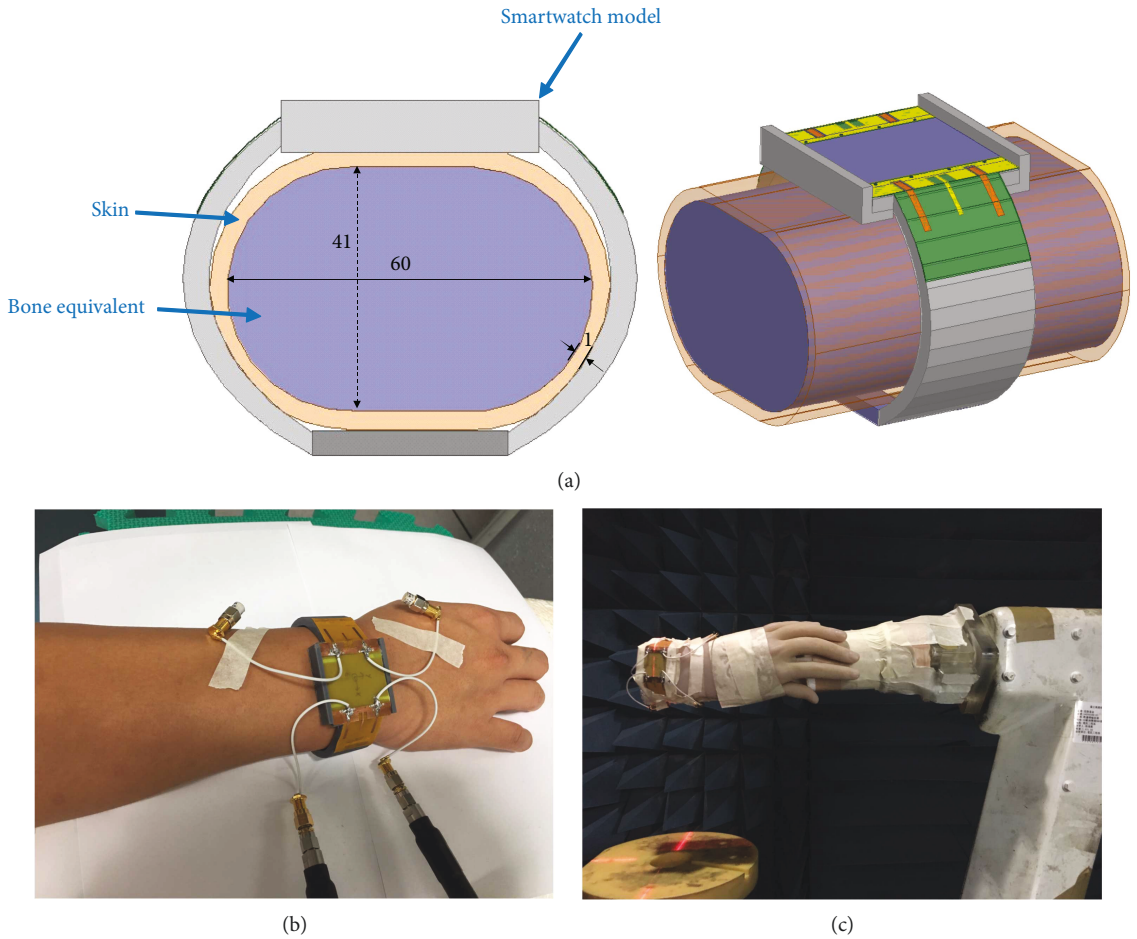

FIGURE 11: (a) Simulation configuration when using a wrist. (b) Photograph of the human wrist measurement. (c) Photograph of the phantom hand measurement in an anechoic chamber.

a wrist model, measurement is conducted by using a phantom hand, and measurement is conducted by using a human wrist. The S_{11} obtained from measurement and simulation are less than −6 dB in the 5.2–5.84 GHz band. The S_{21}, S_{31}, and S_{41} obtained from measurement and simulation are less than −20 dB in the 5.2–5.84 GHz band. The S_{11}, S_{21}, and S_{31}

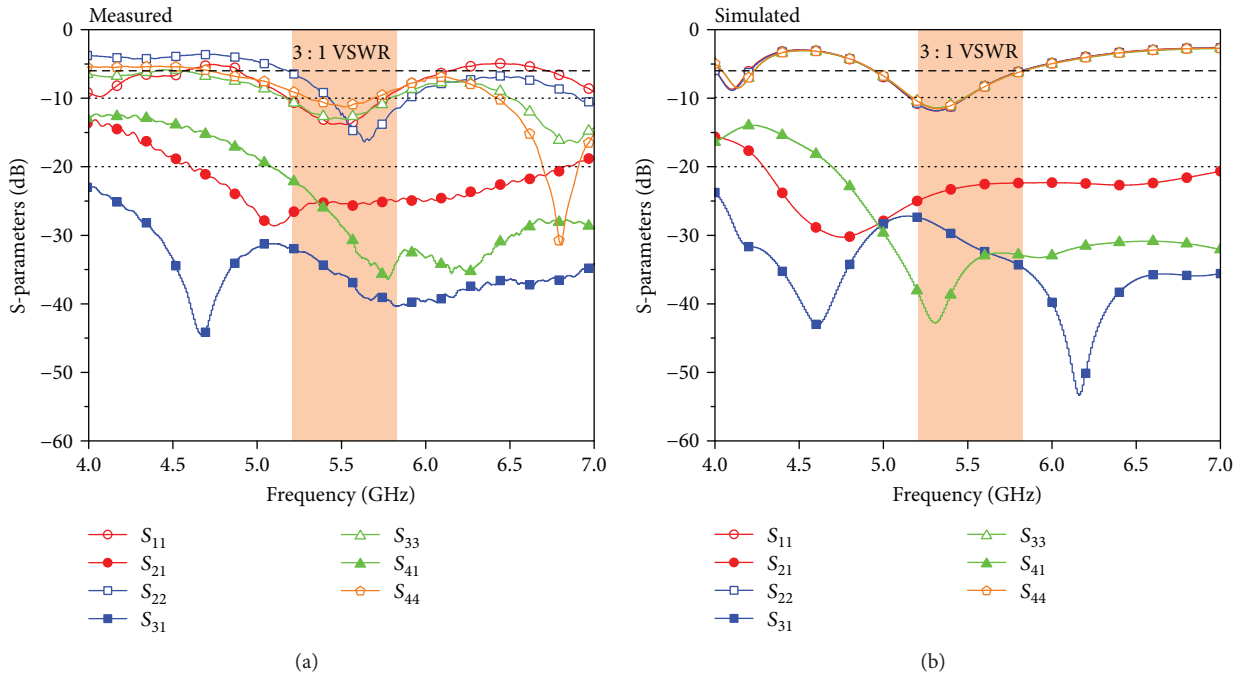

FIGURE 12: (a) Measured S-parameters for the four-element MIMO antennas with a human wrist and (b) simulated ones with the wrist model.

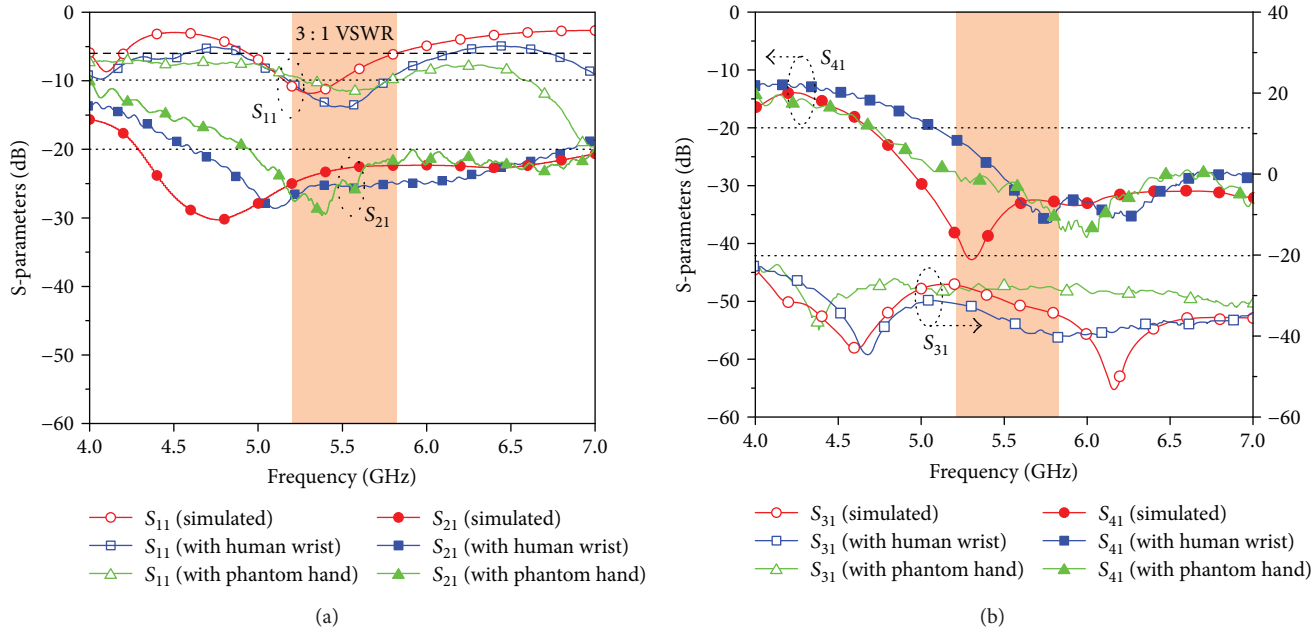

FIGURE 13: Comparison of the S-parameters obtained when simulation is conducted by using a wrist model, measurement is conducted by using a phantom hand, and measurement is conducted by using a human wrist: (a) *S*11 and *S*21 and (b) *S*31 and *S*41.

measured with the phantom hand are similar to those measured with the human wrist. Nevertheless, S_{21} and S_{41} have slight frequency shifts between the simulated and measured results, which may be due to the 50 Ω mini coaxial lines that are not included in the simulation or in the variation of the bending of the antenna. However, the simulated S_{21} and S_{41} parameters are also lower than −20 dB in the 5.2–5.84 GHz band.

The measured radiation efficiency and peak gain of the four-element MIMO antenna worn on the phantom hand are 45%–55% and 2.2–4 dBi, respectively (Figure 14(a)) over the operational band of 5.2–5.84 GHz. The peak gain varies only slightly over the entire band (5.2–5.48 GHz), with a variation of less than 1.8 dBi. The simulated antenna efficiencies and peak gains for the four-element MIMO antenna with the wrist model are presented in

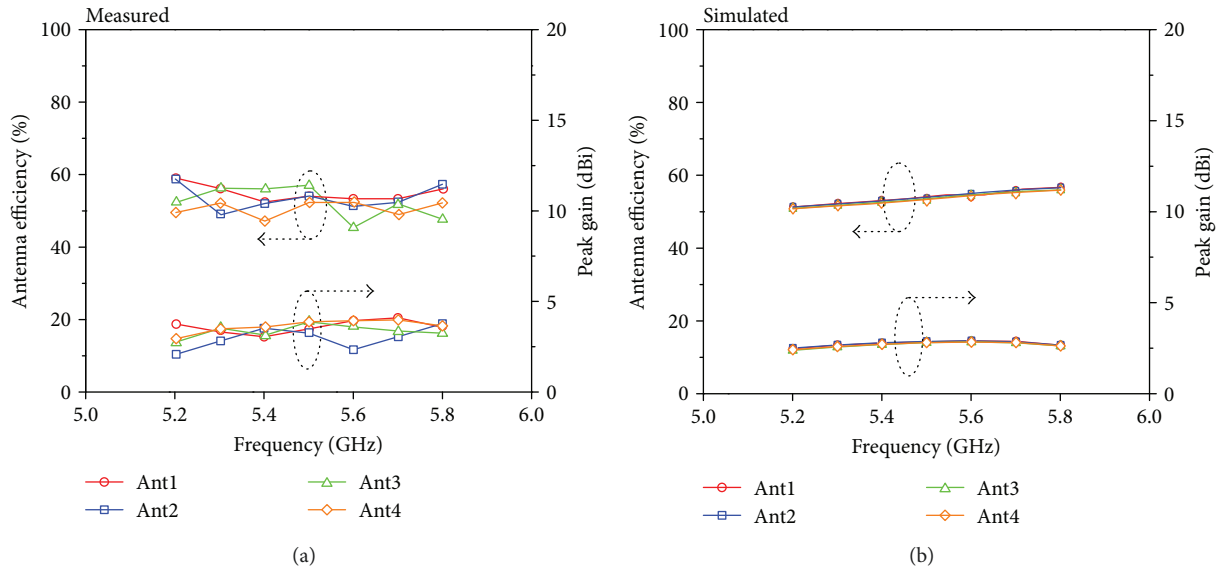

FIGURE 14: (a) Measured antenna efficiency and peak gain for the four-element MIMO antenna worn on the phantom hand; (b) simulated antenna efficiency and peak gain for the four-element MIMO antenna mounted on the wrist.

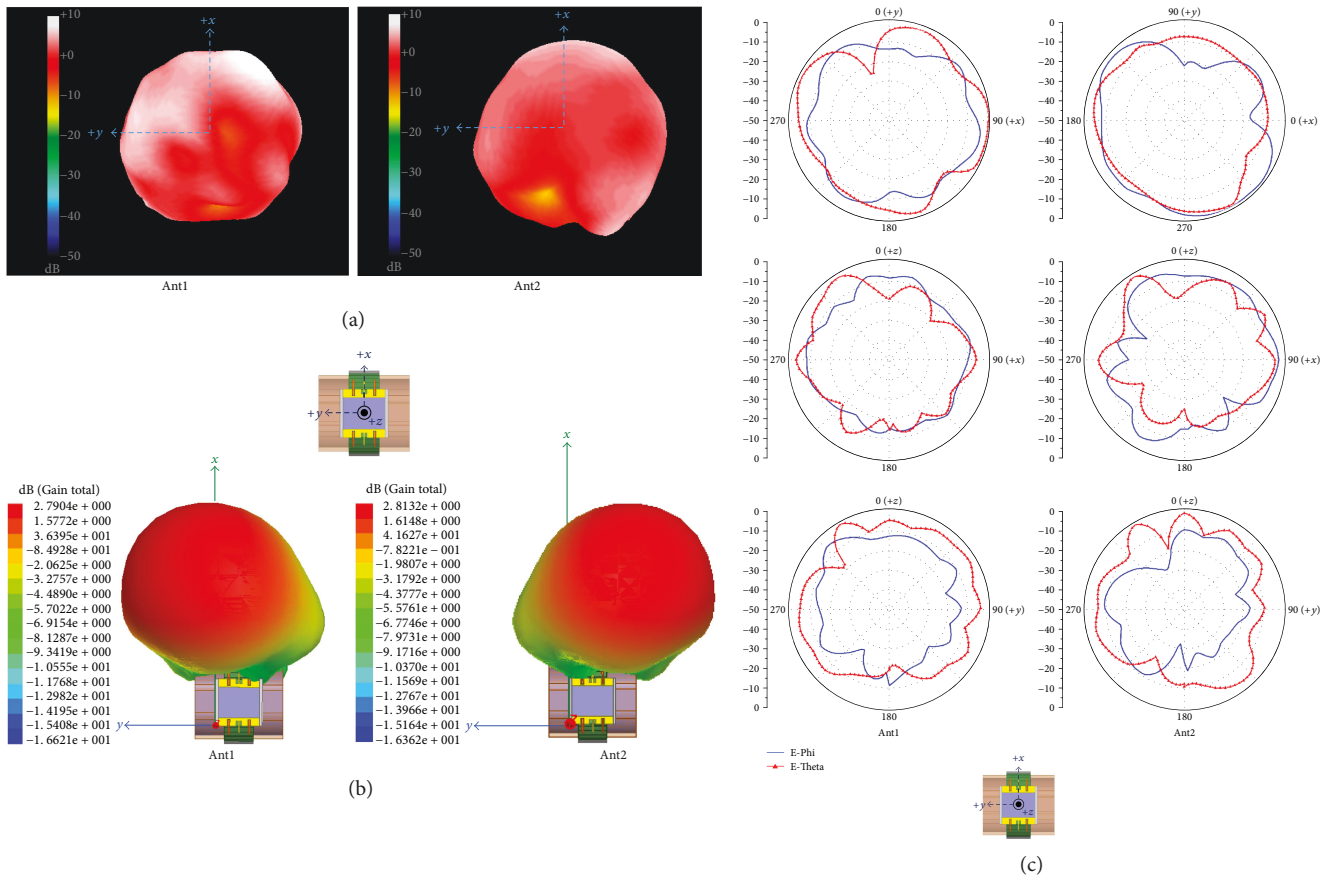

FIGURE 15: (a) Measured antenna 3D radiation patterns for the four-element MIMO antenna worn on the phantom hand. (b) Simulated 3D radiation patterns for the four-element MIMO antenna (at 5.5 GHz) worn on the wrist model. (c) Measured 2D radiation patterns (at 5.5 GHz).

Figure 14(b). The simulated antenna efficiencies are 49%–58% over the operation band, and the simulated peak gains are approximately 2.4–2.9 dBi. The difference between the simulated and measured values in Figures 8 and 14 are observed due to the limitations of the measurement set-up or the flexible substrate variations.

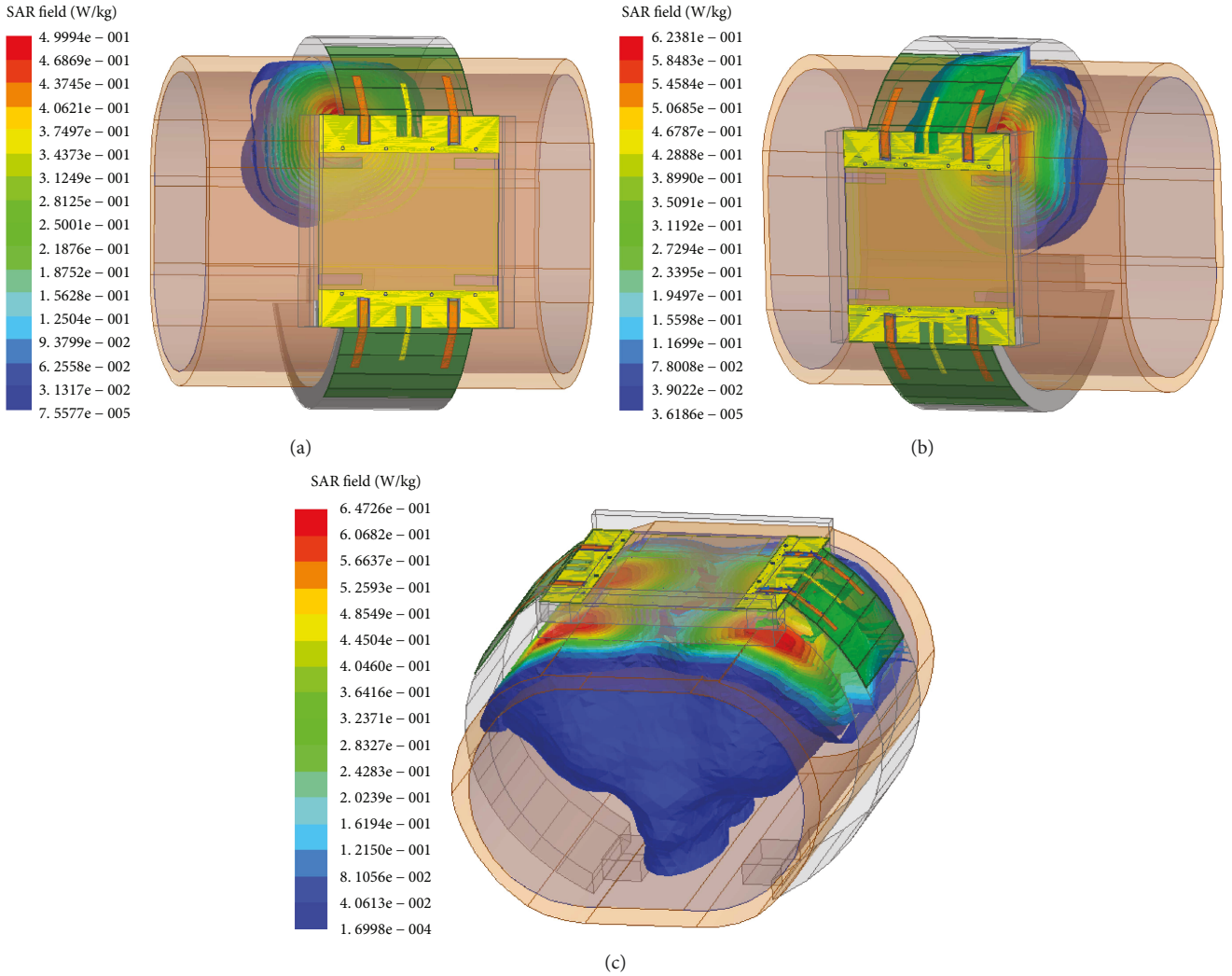

Figure 16: SAR simulation models worn on the wrist (a): Ant1 (b), Ant2 (c), and Ant1–Ant4 (at 5.5 GHz).

The 3D measured radiation pattern at 5.5 GHz for the four-element MIMO antenna on the phantom hand are shown in Figure 15(a). The *XY* plane of Ant1 and Ant2 are displayed. The strongest radiating direction of Ant1 is between the positive *x*-axis and positive *y*-axis and that of Ant2 is between the positive *x*-axis and negative *y*-axis. Figure 15(b) presents the 3D simulated radiation pattern for the four-element MIMO antenna with the wrist model. The radiating direction is affected by the stub and notched block in the ground that is designed between the two elements of the antenna. As a result, the Ant1 and Ant2 simulated radiation patterns are in agreement with the equivalent measured radiation patterns. Figure 15(c) shows the 2D measured radiation patterns for the MIMO antenna on the phantom hand.

In this study, we set the input power of the smartwatch antenna to 18.5 dBm for WiFi applications, which is on the basis of the value used in the MediaTek MT2502 platform for wearables and IoT devices [38]. Figure 16 displays the simulated SAR distributions at 5.5 GHz worn on the wrist. The 10 g SAR value is approximately 0.499 W/kg for Ant1, 0.623 W/kg for Ant2, and 0.647 W/kg for Ant1–Ant4. Both SAR values are less than the corresponding SAR limitations of 4 W/kg, set by the Federal Communications Commission (FCC) [39].

4. Conclusion

This study proposed a novel, compact four-element MIMO antenna for operation at 5.2–5.8 GHz to be used in a smartwatch. This antenna comprises a four-element polyamide antenna that is connected to the system ground and combined with a plastic strap and cover. The manner in which a smartwatch is worn on the wrist affects the functioning of the antenna on the strap. We intend to minimize this effect; therefore, three methods are employed in this paper to investigate the effect on the antenna—simulation by using a wrist model, measurement by using a phantom hand, and measurement by using a human wrist. The measured and simulated S_{11} are less than −6 dB in the 5.2–5.84 GHz band. The measured and simulated S_{21}, S_{31}, and S_{41} are less than −20 dB in the 5.2–5.84 GHz band. The proposed MIMO antenna has superior isolation because a stub and notched block in the antenna ground

and the slit in the system ground are used. The maximum measured antenna efficiency for the four-element MIMO antenna in free space is approximately 97%. This value reduces to 55% when the MIMO antenna is worn on the hand. The maximum measured antenna peak gain reduces from 5.6 to 4 dBi when the antenna is worn on the hand. The radiating direction of Ant1 is between the positive x-axis and the positive y-axis, whereas that of Ant2 is between the positive x-axis and the negative y-axis. Moreover, the antenna elements exhibited excellent ECC values, which indicate favorable isolation of the communication channels. The proposed MIMO antenna is well integrated and suitable for use in the watchstrap of a smartwatch.

Conflicts of Interest

The authors declare that they have no conflicts of interest.

Acknowledgments

This study was supported by the Antenna & Microwave Engineering Laboratory, National Kaohsiung Marine University, Taiwan. This manuscript was edited by Wallace Academic Editing.

References

[1] S. I. Kwak, D. U. Sim, J. H. Kwon, and Y. J. Yoon, "Design of PIFA with metamaterials for body-SAR reduction in wearable applications," *IEEE Transactions on Electromagnetic Compatibility*, vol. 59, no. 1, pp. 297–300, 2017.

[2] M. A. Chung and C. F. Yang, "Built-in antenna design for 2.4 GHz ISM band and GPS operations in a wrist-worn wireless communication device," *IET Microwaves Antennas & Propagation*, vol. 10, no. 12, pp. 1285–1291, 2016.

[3] S.-W. Su and C.-T. Lee, "Metal-frame GPS antenna for smartwatch applications," *Progress in Electromagnetics Research Letters*, vol. 62, pp. 41–47, 2016.

[4] C. Y. Chiu and R. D. Murch, "Watch-sized four-port dual-band MIMO antennas," in *2016 IEEE-APS Topical Conference on Antennas and Propagation in Wireless Communications (APWC)*, pp. 1–4, Cairns, QLD, Australia, September 2016.

[5] W. S. Chen, G. Q. Lin, and W. H. Hsu, "WLAN MIMO antennas with a GPS antenna for smart watch applications," in *2017 International Workshop on Electromagnetics: Applications and Student Innovation Competition*, pp. 89-90, London, UK, May-June 2017.

[6] W. S. Chen, C. K. Yang, and W. S. Sin, "MIMO antenna with Wi-Fi and blue-tooth for smart watch applications," in *2015 IEEE MTT-S 2015 International Microwave Workshop Series on RF and Wireless Technologies for Biomedical and Healthcare Applications (IMWS-BIO)*, pp. 212-213, Taipei, Taiwan, September 2015.

[7] M. Jeon, W. C. Choi, and Y. J. Yoon, "GPS, bluetooth and Wi-Fi tri-band antenna on metal frame of smartwatch," in *2016 IEEE International Symposium on Antennas and Propagation (APSURSI)*, pp. 2177-2178, Fajardo, PR, USA, June-July 2016.

[8] G. S. Li, G. Gao, J. H. Bao, B. Yi, C. Y. Song, and L. A. Bian, "A watch strap antenna for the applications of wearable systems," *IEEE Access*, vol. 5, pp. 10332–10338, 2017.

[9] Z. H. Jiang, D. E. Brocker, P. E. Sieber, and D. H. Werner, "A compact, low-profile metasurface-enabled antenna for wearable medical body-area network devices," *IEEE Transactions on Antennas and Propagation*, vol. 62, no. 8, pp. 4021–4030, 2014.

[10] J. Lee, S. I. Kwak, and S. Lim, "Wrist-wearable zeroth-order resonant antenna for wireless body area network applications," *Electronics Letters*, vol. 47, no. 7, pp. 431-432, 2011.

[11] B. Hu, G. P. Gao, L. L. He, X. D. Cong, and J. N. Zhao, "Bending and on-arm effects on a wearable antenna for 2.45 GHz body area network," *IEEE Antennas and Wireless Propagation Letters*, vol. 15, pp. 378–381, 2016.

[12] Q. H. Abbasi, M. Ur Rehman, X. D. Yang, A. Alomainy, K. Qaraqe, and E. Serpedin, "Ultrawideband band-notched flexible antenna for wearable applications," *IEEE Antennas and Wireless Propagation Letters*, vol. 12, pp. 1606–1609, 2013.

[13] P. Gao, S. He, X. B. Wei, Z. Q. Xu, N. Wang, and Y. Zheng, "Compact printed UWB diversity slot antenna with 5.5-GHz band-notched characteristics," *IEEE Antennas and Wireless Propagation Letters*, vol. 13, pp. 376–379, 2014.

[14] T. S. P. See and Z. N. Chen, "An ultrawideband diversity antenna," *IEEE Transactions on Antennas and Propagation*, vol. 57, no. 6, pp. 1597–1605, 2009.

[15] G. Srivastava and A. Mohan, "Compact MIMO slot antenna for UWB applications," *IEEE Antennas and Wireless Propagation Letters*, vol. 15, pp. 1057–1060, 2016.

[16] S. A. Zhang, Z. N. Ying, J. Xiong, and S. L. He, "Ultrawideband MIMO/diversity antennas with a tree-like structure to enhance wideband isolation," *IEEE Antennas and Wireless Propagation Letters*, vol. 8, pp. 1279–1282, 2009.

[17] M. A. Antoniades and G. V. Eleftheriades, "A compact multiband monopole antenna with a defected ground plane," *IEEE Antennas and Wireless Propagation Letters*, vol. 7, pp. 652–655, 2008.

[18] C. M. Luo, J. S. Hong, and L. L. Zhong, "Isolation enhancement of a very compact UWB-MIMO slot antenna with two defected ground structures," *IEEE Antennas and Wireless Propagation Letters*, vol. 14, pp. 1766–1769, 2015.

[19] S. W. Su, C. T. Lee, and F. S. Chang, "Printed MIMO-antenna system using neutralization-line technique for wireless USB-dongle applications," *IEEE Transactions on Antennas and Propagation*, vol. 60, no. 2, pp. 456–463, 2012.

[20] S. Zhang and G. F. Pedersen, "Mutual coupling reduction for UWB MIMO antennas with a wideband neutralization line," *IEEE Antennas and Wireless Propagation Letters*, vol. 15, pp. 166–169, 2016.

[21] Q. Li, A. P. Feresidis, M. Mavridou, and P. S. Hall, "Miniaturized double-layer EBG structures for broadband mutual coupling reduction between UWB monopoles," *IEEE Transactions on Antennas and Propagation*, vol. 63, no. 3, pp. 1168–1171, 2015.

[22] M. Karaboikis, C. Soras, G. Tsachtsiris, and V. Makios, "Compact dual-printed inverted-F antenna diversity systems for portable wireless devices," *IEEE Antennas and Wireless Propagation Letters*, vol. 3, pp. 9–14, 2004.

[23] R. Karimian, H. Oraizi, S. Fakhte, and M. Farahani, "Novel F-shaped quad-band printed slot antenna for WLAN and WiMAX MIMO systems," *IEEE Antennas and Wireless Propagation Letters*, vol. 12, pp. 405–408, 2013.

[24] C. M. Lee and C. W. Jung, "Radiation-pattern-reconfigurable antenna using monopole-loop for Fitbit Flex wristband," *IEEE*

Antennas and Wireless Propagation Letters, vol. 14, pp. 269–272, 2015.

[25] P. Thongbor, A. Ruengwaree, V. Pirajnanchai, W. Naktong, and N. Fhafhiem, "Rectangular monopole antenna with arrow-shaped slot etching for UWB-MIMO application," in *2016 13th International Conference on Electrical Engineering/Electronics, Computer, Telecommunications and Information Technology (Ecti-Con)*, pp. 1–4, Chiang Mai, Thailand, June-July 2016.

[26] "HFSS 15 Hfss Onlinehelp Ansoft Corp., (undated)".

[27] M. S. Sharawi, "Current misuses and future prospects for printed multiple-input, multiple-output antenna systems [wireless corner]," *IEEE Antennas and Propagation Magazine*, vol. 59, no. 2, pp. 162–170, 2017.

[28] K. L. Wong, J. Y. Lu, L. Y. Chen, W. Y. Li, and Y. L. Ban, "8-antenna and 16-antenna arrays using the quad-antenna linear array as a building block for the 3.5-GHz LTE MIMO operation in the smartphone," *Microwave and Optical Technology Letters*, vol. 58, no. 1, pp. 174–181, 2016.

[29] Y. L. Ban, C. Li, C. Y. D. Sim, G. Wu, and K. L. Wong, "4G/5G multiple antennas for future multi-mode smartphone applications," *IEEE Access*, vol. 4, pp. 2981–2988, 2016.

[30] W. Y. Li, W. Chung, F. R. Hsiao, T. H. Kao, and M. C. Huang, "Conformai integrated multi-layer thin-film antenna by novel LITA technologies for smartwatch wearable device applications," in *2016 International Symposium on Antennas and Propagation (ISAP)*, pp. 22-23, Okinawa, Japan, October 2016.

[31] D. Wen, Y. Hao, H. Wang, and H. Zhou, "A wearable antenna design using a high impedance surface for all-metal smartwatch applications," in *2017 International Workshop on Antenna Technology: Small Antennas, Innovative Structures, and Applications (iWAT)*, pp. 274–276, Athens, Greece, March 2017.

[32] S. W. Su and Y. T. Hsieh, "Integrated metal-frame antenna for smartwatch wearable device," *IEEE Transactions on Antennas and Propagation*, vol. 63, no. 7, pp. 3301–3305, 2015.

[33] D. Wu and S. W. Cheung, "A cavity-backed annular slot antenna with high efficiency for smartwatches with metallic housing," *IEEE Transactions on Antennas and Propagation*, vol. 65, no. 7, pp. 3756–3761, 2017.

[34] A. B. Chhabra and A. M. Freilich, *Regional anatomy and surgical intervals*, chapter 4 wrist and hand, Elsevier, 2015.

[35] A. V. Vorst, A. Ro, and Y. Kotsuka, *RF/Microwave Interaction with Biological Tissues*, John Wiley & Sons, Inc., 2006, https://www.wiley.com/en-us/RF+Microwave+Interaction+with+Biological+Tissues-p-9780471732778.

[36] A. T. Mobashsher and A. M. Abbosh, "Artificial human phantoms: human proxy in testing microwave apparatuses that have electromagnetic interaction with the human body," *IEEE Microwave Magazine*, vol. 16, no. 6, pp. 42–62, 2015.

[37] U. Ali, S. Ullah, J. Khan et al., "Design and SAR analysis of wearable antenna on various parts of human body, using conventional and artificial ground planes," *Journal of Electrical Engineering and Technology*, vol. 12, no. 1, pp. 317–328, 2017.

[38] *MT2502 Chipset Technical Brief*, MediaTek Ltd., Hsinchu, Taiwan, 2014, https://labs.mediatek.com/en/chipset/MT2502.

[39] *47498 D01 General RF Exposure Guidance v06, RF Exposure Procedures and Equipment Authorization Policies for Mobile and Portable Devices*, Federal Communications Commission, Washington, DC, USA, 2015.